CEAS-GNC-2024-044

EuroGNC Navigation Guidance Control CEAS Bristol, UK June 11th-13th 2024
University of BRISTOL ROYAL AERONAUTICAL SOCIETY AIAA

Robust Control Design for a Sub-Orbital Launch Vehicle with Destabilizing Sloshing Dynamics

João Belfo GNC Engineer, DEIMOS Engenharia SA, GNC Competence Center, 1070-061, Lisbon, Portugal. joao.belfo@deimos.com.pt

Nicola Somma GNC Engineer, DEIMOS Engenharia SA, GNC Competence Center, 1070-061, Lisbon, Portugal. nicola.somma@elecnor.es

Alejandro Montero GNC Engineer, DEIMOS Space UK, GNC Competence Center, Harwell Oxford Didcot, United Kingdom. alejandro.montero@elecnor.es

Paulo Rosa Head of the Avionics Business Unit, DEIMOS Engenharia SA, 1070-061, Lisbon, Portugal. paulo.rosa@deimos.com.pt

João Santos Instrumentation Engineer, OMNIDEA Lda, 2825-149 Caparica, Portugal. joao.santos@omnidea.net

Tiago Moreira System Engineer, OMNIDEA Lda, 2825-149 Caparica, Portugal. tiago.moreira@omnidea.net

Pedro Simplício GNC Engineer, Aurora Technology for the European Space Agency, ESTEC, Noordwijk, The Netherlands. pedro.simplicio@ext.esa.int

António Rinalducci GNC System Engineer, European Space Agency, ESTEC, Noordwijk, The Netherlands. antonio.rinalducci@esa.int

Yohann Torres Chemical Propulsion Engineer, European Space Agency, Noordwijk, The Netherlands. yohann.torres@esa.int

ABSTRACT

This paper addresses the attitude tracking control problem for an experimental sub-orbital vehicle, with destabilizing fuel sloshing dynamics and limited actuation bandwidth. As part of the control design process, a Linear Time-Invariant (LTI) model, including the rigid-body translational and rotational dynamics, as well as fuel sloshing dynamics, is thoroughly formulated, validated, and then ultimately used for controller synthesis and analysis. A stability analysis is performed confirming the destabilizing sloshing dynamics present in the vehicle considered. To address this problem, a set of filters is included in the structure of the controller, with the associated parameters being tuned by solving a non-smooth optimization problem. Gain and phase margins, as well as Monte-Carlo (MC) results obtained by using a high-fidelity Functional Engineering Simulator (FES), demonstrate that the controller meets the desired levels of performance and robustness.

Keywords: Robust Control Design; Unstable Sloshing dynamics;

Nomenclature

Φ, Θ, Ψ	=	Euler angles (roll, pitch, yaw)
p, q, r	=	Euler angles rates (roll rate, pitch rate, yaw rate)
$\dot{Y}, \dot{Z}$	=	Linear velocities perturbations (drift-Y, drift-Z)
F_a	=	Aerodynamic force
M	=	torque
T	=	thrust
D	=	drag
m	=	mass
V	=	velocity
I_{xx}, I_{yy}, I_{zz}	=	inertia along x, y, and z axis
k	=	stiffness
c	=	damping
CoG	=	Centre of Gravity
x_{TVC}	=	distance between TVC position and CoG
x_a	=	distance between the center of pressure position and CoG
LOX	=	Liquid Oxidizer
LNG	=	Liquified Natural Gas (Fuel)
IMU	=	Inertial Measurement Unit
$GNSS$	=	Global Navigation Satellite System

1 Introduction

In the context of an ESA-sponsored project under the GSTP program, Omnidea is currently engaged in the activity Portuguese Enabling Technologies and Building Blocks – Phase 2, aiming to develop technology building blocks that will demonstrate technologies for potential utilization in small launcher applications. In particular, an experimental sub-orbital vehicle (SoV) is being developed as a means to bolster the development of key technologies by the Portuguese industry and establish integration capabilities. In this context, DEIMOS is responsible for the development of a Functional Engineering Simulator (FES), and for the preliminary design, implementation, and analysis of a Guidance, Navigation, and Control (GNC) subsystem. Given that the project is in its early stages where the system management and design of the vehicle is still in progress, the development of the GNC should take this into account and contribute with inputs to the system definition and design, for instance, in terms of control authority and stability analysis. The FES corresponds to a nonlinear, high-fidelity simulator, including effects such as the Thrust Vector Control (TVC) nonlinear actuator model, the Reaction Control System (RCS) nonlinear actuator model, fuel sloshing, aerodynamics, Tail-Wags-Dog (TWD) effect, Mass, Center-of-gravity, and Inertia (MCI) model, and environment and perturbation models (e.g., wind turbulence and atmosphere models).

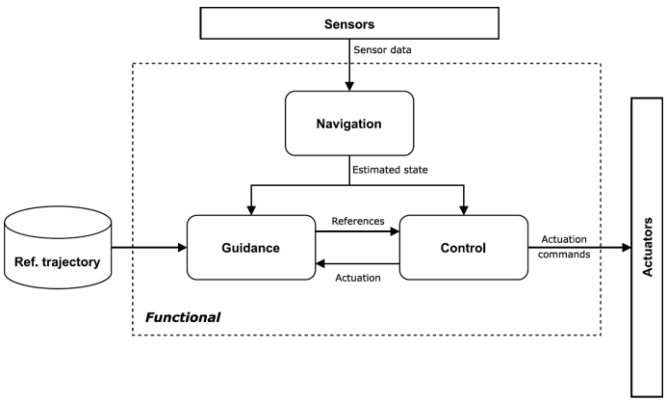

Fig. 1 GNC architecture

All the models have been either developed and validated during the project or inherited from internal DEIMOS libraries.

Besides providing inputs from controllability analysis to the system, the main challenge for the development of the GNC is the control design considering the fuel sloshing effect. Other effects, such as flexibility, were deemed to have a smaller impact on the dynamics, given the relatively short length (approximately 6 m) of the vehicle. The Guidance function consists in a Look-Up-Table (LUT) indexed by the non-gravitational velocity, providing the three Euler angles representing the reference attitude. The angles are then compared to the estimates from Navigation, yielding the angle error that is then fed to the controller, which is responsible for commanding the TVC deflection angles and the RCS ON/OFF commands (see figure 1).

This paper is organized as follows: the problem is formulated in section 2; the control design is presented in section 3 – first the general design approach is presented, followed by the LTI generation and validation. The control synthesis is presented next and the obtained controllers are analyzed and tested in the FES.

2 Problem Formulation

A small experimental sub-orbital vehicle, with 5.497 m of length and 1 m of diameter, as illustrated in figure 2, with the body frame located at the tip of the nose cone (x-axis being the longitudinal axis), and both oxidizer and fuel tanks located on top and below the total center of mass, CoG, of the vehicle, respectively, being the fuel tank closer to the CoG. The FES includes a model of the vehicle together with the given specific aerodynamics and MCI data. The FES also contains several other high-fidelity models/effects such as the atmosphere, wind and turbulence, TWD, TVC, RCS, GNSS and IMU, and fuel sloshing.

Fig. 2 Diagram of the vehicle

The problem can now be formulated as follows: given the nonlinear model implemented in the FES, that receives the TVC and RCS actuation signals and outputs the current vehicle state as measured by the GNSS and IMU sensors, compute the actuation signals such that a predefined trajectory is followed.

For the ascent trajectory considered in this activity, the Guidance was implemented as an LUT that outputs the reference trajectory. The Navigation is such that it estimates the vehicle state from the sensors measurements with a given accuracy. Finally, the Controller is designed such that the reference trajectory can be followed and pre-defined levels of performance and robustness are attained. This paper only addresses the Control problem, assuming that the other components, in particular the Navigation function, perform withing the desired specifications.

3 Control Design

3.1 Controller Design approach

This section describes the controller synthesis approach adopted in this paper, which is based on robust control theory applied to launcher GNC, exploiting the advances of the last decade in this field [3][4]. The process starts with the linearization of the dynamics, which are then validated against the nonlinear models using the FES, with the latter being a key step in the control design process. These linearized models are used, together with the dynamic weights (design tuning nobs), in the design interconnection for the controller synthesis.

For the problem presented in this paper, an H_∞ control design approach was selected, given that H_∞ constraints are suitable to ensure robust stability and performance for families of plants typically described in a Linear Fractional Transformation (LFT) fashion. The overall controller synthesis methodology can be structured into the following three main steps:

- Modelling: The model adopted within the work reported in this document is described by a sequence of analytical LTI models, which are then validated against the nonlinear dynamics. Some of the LTI's parameters are set to be uncertain, according to the time evolution of the nonlinear dynamics in the FES.
- Controller synthesis: This step is where the controller is actually computed by using, in this case, an H_∞ control design approach (e.g., using routines such as *systune* in MATLAB® [10]).
- Analysis: The closed-loop system is finally evaluated with the controller obtained in the previous step. It is typically beneficial to iterate between these last two steps, either manually or by using (global) optimization approaches.

The first step in the design of the controller is the selection of the dynamic weights or performance goals. The selection is typically done based on knowledge regarding the exogenous disturbances acting on the system, as well as on the measurement noise, actuator dynamics and constraints, and desired performance levels. In figure 3, the interconnection used to synthesize the controller based on the minimization of the norm of the transfer functions is depicted. The interfaces of the system are as follows:

- The inputs and outputs of the Δ block modelling the uncertainties (this is used only for performance and robustness analyses; the nominal values of the plant are used for synthesis);
- The input and output of the Δ delay block modelling the systems delays from sensors, Navigation algorithm, and actuation;
- The noise blocks, modeling the sensor noises;
- The disturbances (exogeneous inputs), modeling perturbations that are added as inputs to the system through the same channel as the commands, such as actuator imperfections, etc.;
- The performance outputs.

The signals feeding into, and coming out of, the system is weighted according to their physical meaning. These weights are applied to the disturbances at the input of the plant, the noise of the measurements, the control commands and over the performance outputs.

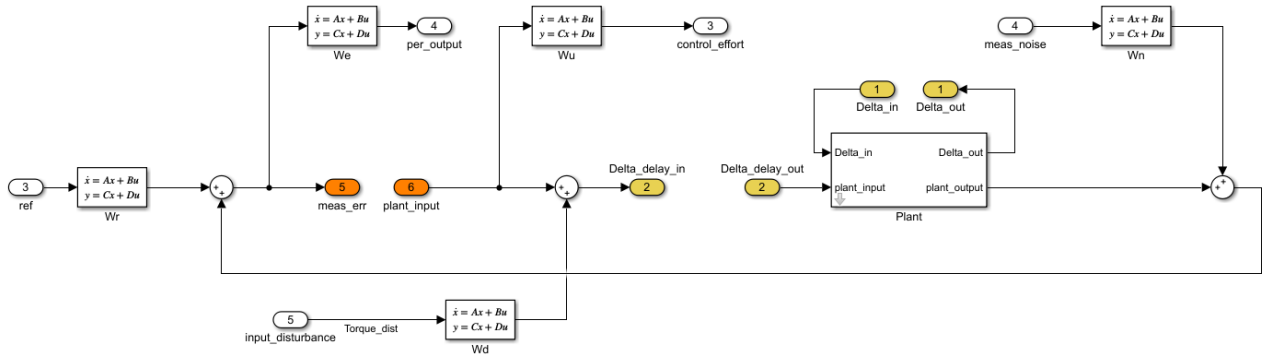

Fig. 3 Controller synthesis interconnection

Once the interconnection is formulated, an optimization problem is solved so as to minimize the gain from the selected inputs (disturbances and measurement noise, and possibly outputs of a delta-block, representing model uncertainty, and delta-delay-block, representing uncertain delays in the system) to the desired performance outputs.

For the purpose of the controller synthesis, the wind turbulence and sloshing disturbances are considered the most relevant perturbations to the controller behavior. Observing their impact in the nonlinear system, the magnitude of the corresponding disturbance is in the order of magnitude of hundreds of Nm, the sloshing adding a disturbance in the sloshing frequency around 1.1Hz and the wind turbulence being modeled as a disturbance with an approximately constant level at all frequencies. This motivated the selection of a constant disturbance dynamic weight W_d with 100 Nm low frequency gain. The actuator model contributes also with a delay that is added to the delays of the system and used in the control design, considering a Padé approximation.

Regarding noise, it was observed that the signal computed by Navigation entailed an error of magnitude around 0.1 degrees. Therefore, a constant weight for angular noise of magnitude 0.1 degrees and a high pass transfer function weight for the angular rate noise are used in the control design. The measurement also contributes with a delay that is also added to the overall delay impacting on the system.

3.2 LTI Generation and Validation

In order to perform a robust control design for the GNC subsystem, a Linear Time Invariant (LTI) representation of the model implemented in the FES was required. The derivation of a reliable LTI is of paramount importance for the control design process, justifying the need of an in-depth validation against the nonlinear simulator. In this section, the process of generating the LTI representation of the nonlinear dynamics through the analytical equations is briefly mentioned. Since the development of the LTI require the linearization, i.e., the linear approximation, of highly nonlinear functions, the linearization error can become large after a few seconds of comparison. To tackle this problem, a sequence of LTIs is generated by sampling the LTI's parameters time evolution during a nominal FES simulation. The validation is then performed at different linearization times along the trajectory by applying a perturbation at a given time and comparing the evolution of the states from the nonlinear simulation and from the LTI, for the same input. It is remarked that the full derivation of the LTI model is not presented here for the sake of brevity.

The generation of the LTI starts from the linear and angular momentum conservation equations, assuming zero reference angular velocity and small linear and angular velocity perturbations, and it uses the small angle approximation to derive the linear system given by

$$\dot{x}_n = A_n x_n + B_n u_{ext}\,, \quad y_n = C_n x_n \tag{1}$$

where $x_n = [\dot{Y}, \dot{Z}, \Phi, \Theta, \Psi, \mathrm{p}, \mathrm{q}, \mathrm{r}]$ is the state composed by the lateral drifts, the attitude angles and angle rates, u_{ext} corresponds to the actuation torques, i.e., the torques generated by the TVC and RCS actuation, and

$$A_n = \begin{bmatrix} -\frac{F_a}{V\,m} & 0 & 0 & 0 & \frac{F_a+T-D}{m} & 0 & 0 & -\frac{F_a x_a}{V\,m} \\ 0 & -\frac{F_a}{V\,m} & 0 & -\frac{F_a+T-D}{m} & 0 & 0 & \frac{F_a x_a}{V\,m} & 0 \\ 0 & 0 & 0 & 0 & 0 & 1 & 0 & 0 \\ 0 & 0 & 0 & 0 & 0 & 0 & 1 & 0 \\ 0 & 0 & 0 & 0 & 0 & 0 & 0 & 1 \\ 0 & 0 & 0 & 0 & 0 & 0 & 0 & 0 \\ 0 & \frac{F_a x_a}{V\,I_{yy}} & 0 & \frac{F_a x_a}{I_{yy}} & 0 & 0 & -\frac{F_a x_a^2}{V\,I_{yy}} & 0 \\ -\frac{F_a x_a}{V\,I_{zz}} & 0 & 0 & 0 & \frac{F_a x_a}{I_{zz}} & 0 & 0 & -\frac{F_a x_a^2}{V\,I_{zz}} \end{bmatrix}, B_n = \begin{bmatrix} 0 & 0 & -\frac{1}{m\,x_{TVC}} \\ 0 & \frac{1}{m\,x_{TVC}} & 0 \\ 0 & 0 & 0 \\ 0 & 0 & 0 \\ 0 & 0 & 0 \\ \frac{1}{I_{xx}} & 0 & 0 \\ 0 & \frac{1}{I_{yy}} & 0 \\ 0 & 0 & \frac{1}{I_{zz}} \end{bmatrix}$$

with C_n selecting the state signals to be monitored. By discarding the firsts two states, the rotational LTI can be obtained. The sloshing dynamics are given by

$$\dot{x}_s = A_s x_s + B_s u_s + B_{ng} x_n\,, \quad y_s = C_s x_s + D_s U_s' \dot{x}_n + D_s B_{ng}' x_n \qquad (2)$$
$$u_s = U_s \dot{x}_n$$

where $x_s = [x_{LNG}, y_{LNG}, \dot{x}_{LNG}, \dot{y}_{LNG}, x_{LOX}, y_{LOX}, \dot{x}_{LOX}, \dot{y}_{LOX}]$ is the state composed by the sloshing mass displacements and velocities in both fuel and oxidizer tanks. The y_s contains the sloshing forces and torques without any nonlinear terms. The $B_s u_s$ term provides the linear and angular acceleration inputs from the rigid dynamics to the sloshing dynamics, and the $B_{ng} x_n$ (the *ng* stands for non-gravitational) provides the non-gravitational contributions, in particular the torque generated by a longitudinal force acting on the sloshing mass, T_{Lx}, as explained in [1]. This torque is important for the stability analysis presented in the sequel.

To couple the sloshing dynamics in the rigid dynamics, an extra B_n' matrix is developed yielding the rigid dynamics $\dot{x}_n = A_n x_n + B_n u_{ext} + B_n' y_s$. Rearranging the equations, the final augmented LTI model is given by

$$\begin{bmatrix} \delta\dot{x}_n \\ \delta\dot{x}_s \end{bmatrix} = \begin{bmatrix} S^T[A_n B_n D_s B_{ng}'] & S^T[B_n C_s] \\ B_{ng} + B_s U_s S^T[A_n + B_n D_s B_{ng}'] & A_s + B_s U_s S^T B_n C_s \end{bmatrix} \begin{bmatrix} \delta x_n \\ \delta x_s \end{bmatrix} + \begin{bmatrix} B_n \\ B_s U_s B_n \end{bmatrix} \delta u_n \qquad (3)$$

where S^T is the transpose of the matrix $S = I - B_n D_s U_s'$.

Given this formulation, it was possible to decouple pitch and yaw dynamics (roll is not affected by the sloshing), assuming that each of the sloshing mass generates two forces in the body frame (and consequently two torques) that affect pitch and yaw independently. The comparison between the nonlinear attitude angle perturbations and the ones from the LTI are depicted in figure 4 for the pitch angle, for t=50s, which is around the maximum dynamic pressure where the nonlinear dynamics are expected to change faster and, thus, the linearization error is expected to be larger. The plots illustrating the comparison of the drifts and the sloshing mass displacements are also presented.

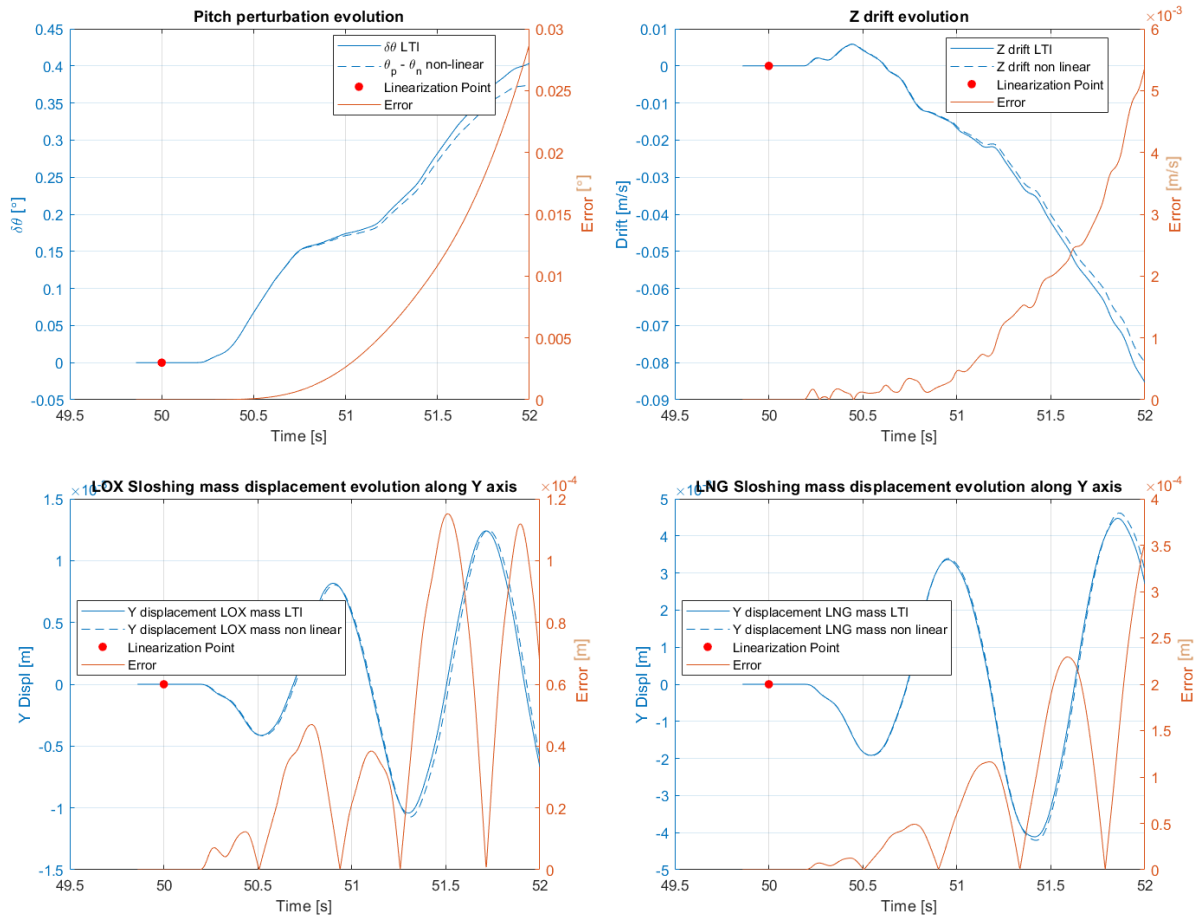

Fig. 4 Pitch perturbation, drift (in body frame), sloshing displacements (in slosh frame), t=50s

At the linearization point, a sinusoidal perturbation is applied to the TVC deflection, in order to affect the translational and rotational dynamics of the vehicle. The perturbation in the TVC deflection has an amplitude 0.5 deg and frequency 1 Hz (close to the sloshing frequency), in order to excite sloshing. The small magnitude of the error even after 2 seconds of simulations demonstrate the reliable representation of the dynamics by the analytical LTI model, that will be then used for the control design, as explained in the following sections.

3.3 Robust Control synthesis

3.3.1 Attitude Controller

The starting point for the controller synthesis is the definition of the dynamic weights used in the design, as mentioned above. Since the actuation to compensate for roll errors is different than for the pitch and yaw errors, the design of the roll attitude controller followed the same strategy and structure, but with

different performance and control effort weights. Furthermore, the sequence of LTI identified and validated in the previous section is now used for the control design. The same approach and structure are used to design the entire LTI sequence's controllers. However, for simplicity, the plots below are obtained from the first LTI model only. The parameters that are set to be uncertain correspond to the MCI parameters, thrust and drag forces, the TVC and Center of Pressure longitudinal positions, and the sloshing masses and spring coefficients.

The preliminary controller structure is a PD (without any additional filters, for the moment), tuned by using *systune*, with the following inputs:

- Tracking error: defined to be the difference between the reference and the measured angle, for which the proportional gain, K_p, is to be optimized.
- Measured angular velocity, for which the gain K_d is to be optimized.

Albeit simple, this control structure is well representative of the industrial state-of-practice [2]. The robust control framework was selected due to the benefits mentioned in section 3.1, especially when additional control requirements (e.g. induced drift and angle of attack) are considered or when rapid missionization (i.e. control retuning for different payloads) is envisaged.

The pitch and yaw controller dynamic weights design are defined as follows. For the present control loop, the performance weight W_e is defined to have a higher penalization to tracking errors larger than 0.5 degrees, with a frequency lower than 0.5Hz. These values were obtained by observing the behavior of the preliminary GNC system: the maximum angular error was around 0.5 degrees, and the reference trajectory variation is relatively slow during the time window around each linearization point and, thus, a bandwidth of 0.5 Hz was considered to be sufficiently wide for the type of signal to be followed.

Using the interconnection illustrated in figure 5 , in which $W_p = blkdiag(W_e, W_u)$, G is the plant model, and K is the controller, it is straightforward to conclude that, if $\left\|\tilde{G}\right\|_\infty < 1$, then

$$\left\|\tilde{G}\right\|_\infty = \left\|W_p \hat{G}\right\|_\infty < 1 \Rightarrow \left\|\hat{G}\right\|_\infty < \frac{1}{\left\|W_p\right\|_\infty} \tag{4}$$

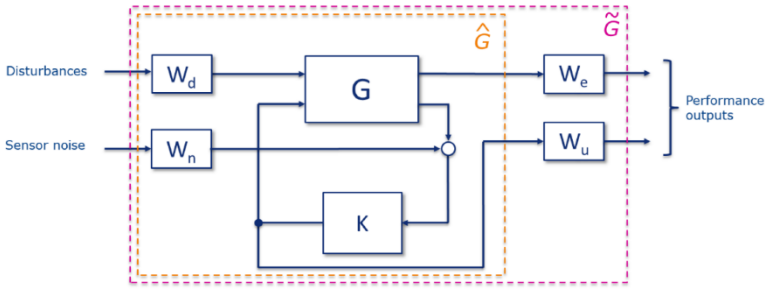

Fig. 5 Simplified interconnection view for controller synthesis

Hence, the closed-loop system is compliant with the requirements, embedded in W_p and in the augmented $\tilde{G}$ plant. For this case, W_u is defined so that the range of torques that can be generated is such that it can counteract, at least, the aerodynamic torque. Therefore, observing that the range of aerodynamic torques in a nominal simulation has a maximum value of 2,000 Nm, W_u is then defined as a constant set to 5e-04, so that a 1-degree tracking error generates a torque command smaller than 2,000 Nm, thus keeping the actuators sufficiently far from the saturation – the saturation can be computed with the maximum allowed TVC angle of 8 degrees and with the average thrust level, yielding a maximum torque around 9,000 Nm.

From figures 6 and 7, it is possible to observe that the requirements in terms of tracking error and maximum control effort are satisfied in this case, for the nominal system, being the uncertain system analyzed in the sequel. The blue line corresponds to the singular value of the transfer function from disturbances and noise to the input of the W_e weight. Since this weight is fed by the tracking error, and

the physical system (vehicle) behaves as a low-pass filter, very high-frequency disturbances do not impact this tracking error. Hence, there is no feedthrough from disturbances to this output channel, thus justifying the shape of the plot.

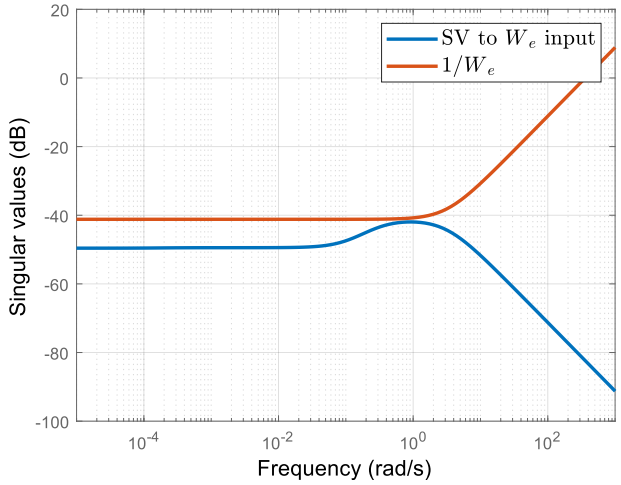

Fig. 6 Singular values of the transfer function from exogenous inputs to tracking error performance VS requirement (pitch & yaw)

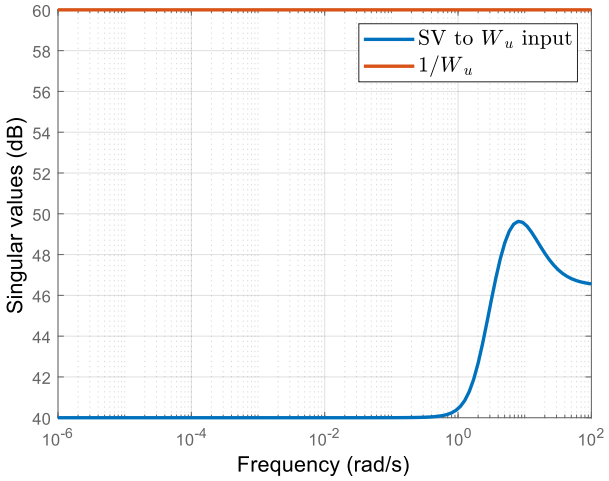

Fig. 7 Singular values of the transfer function from exogenous inputs to control effort VS requirement (pitch & yaw)

For the roll attitude controller, the actuation is done through the RCS. The W_u weight for roll control should be different from the one for yaw and pitch because (1) the disturbances affecting roll are relatively small when compared to the ones affecting pitch and yaw, and (2) the RCS generates torques one order of magnitude lower than those from the TVC. The W_u weight is defined as a constant set to 0.02, so that a 1-degree tracking error generates a torque smaller than 50 Nm, which is approximately the torque that RCS can provide. The W_e for the roll controller synthesis is defined to have a constant penalization to tracking errors higher than 3 degrees. Initially, this value was the same as for the pitch and yaw controller. However, since the driving requirement for roll control is on the maximum roll rate of 10 deg./s, it is not necessary to have a higher penalization on the angle. Figures 8 and 9 depict the transfer functions from the exogenous inputs to tracking error performance and control effort, and the respective requirements.

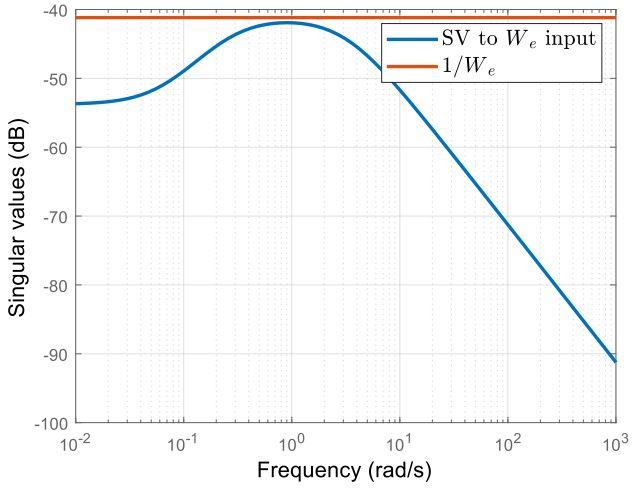

Fig. 8 Singular values of the transfer function from exogenous inputs to tracking error performance VS requirement (roll)

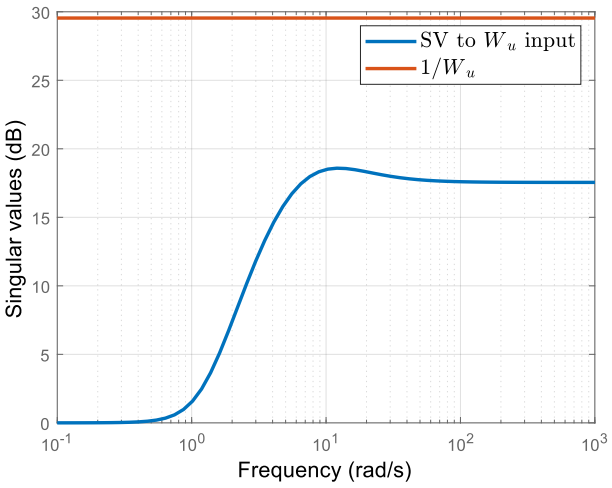

Fig. 9 Singular values of the transfer function from exogenous inputs to control effort VS requirement (roll)

Considering the above-mentioned approach, structure and dynamic weights, and using the rotational LTI model coupled with sloshing LTI for the controller synthesis, the preliminary rigid+sloshing controller can be obtained.

In fact, when using the preliminary rigid+sloshing controller described above, the nominal simulation in the FES yielded an unstable result: the sloshing masses oscillate significantly and, at some point, the TVC actuation saturated. This behavior appears when the sloshing torque generated by a longitudinal force acting on the sloshing mass T_{Lx}, mentioned above, is active in the sloshing model implemented in the FES. This result motivated the stability analysis on the LTI side to better understand why the controller obtained previously yields unstable results in the presence of the torque T_{Lx}. For this purpose, and since the sloshing dynamics couples the rotational and translational motion, a more complete LTI representation was developed and validated against the nonlinear model, as described in section 3.2, including the rotational and sloshing dynamics as used before with the addition of the translational dynamics, i.e., the drifts states.

In this analysis, two types of LTI models were generated: an LTI model with translational, rotational, and sloshing dynamics, with and without T_{Lx}. For each of these LTI models, the controller described above was used to generate the corresponding root-locus plots. Figure 10 shows the root-locus of the system composed of the preliminary rigid+sloshing controller and the complete LTI model without the torque T_{Lx} with a zoom in the area of the sloshing poles and zeros, respectively. Figure 11 shows a similar root-locus, but now considering the T_{Lx} with a zoom in the same area. In both figures, the poles and zeros on the top correspond to the oxidizer tank dynamics and the poles and zeros below correspond to the fuel tank dynamics.

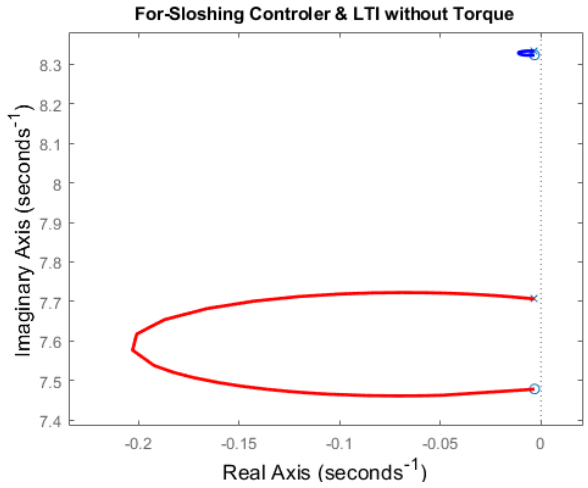

Fig. 10 Root-locus of the controller with LTI not containing the torque T_{Lx}, zoom in

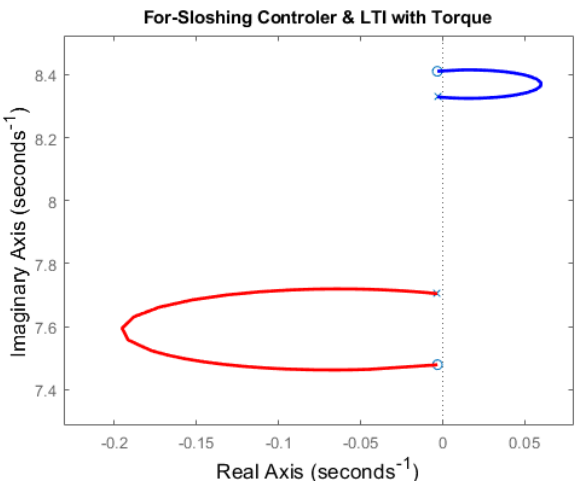

Fig. 11 Root-locus of the controller with LTI containing the torque T_{Lx}, zoom in

As it is apparent in the zoom-in figures, using T_{Lx} in the LTI yielded a root-locus "closing through the right", while without this torque, the root-locus "closes through the left". The consequence of this is that the T_{Lx} yields a closed-loop system that is unstable for most of the controller gain range [5] [6] [7]. In fact, if no damping is considered in the sloshing dynamics, the sloshing poles and zeros will be in the imaginary axis, in which case the root-locus with the T_{Lx} will always be unstable, leading to the conclusion that baffles are required using this structure of a controller [1] [5] [6] [7]. However, in the sloshing model used, there is a small amount of damping and, as it can be observed in the figures, there are some very small and very large root-locus gains that can stabilize, at least, the oxidizer poles. The

main problem is that, if those gains are selected, the preliminary rigid+sloshing performance is either unsatisfactory in terms of angle tracking error, or it saturates the TVC actuation. To address this problem, there are, at least, two possible solutions: (1) one could add baffles to increase sufficiently the damping such that the unstable root-locus arc is mostly to the left of the imaginary axis; (2) designing a specific filter that can add poles and zeros around the unstable sloshing poles and zeros so that these last poles can close to the filter's zeros and vice-versa, i.e., to attract the root-locus curves to the left-hand side. Such a filter is proposed, for instance, in [8], and it has the following structure

$$H(s) = \frac{\omega_d^2}{\omega_n^2} \cdot \frac{s^2 + 2\zeta_n \omega_n s + \omega_n^2}{s^2 + 2\zeta_d \omega_d s + \omega_d^2}\ , \tag{5}$$

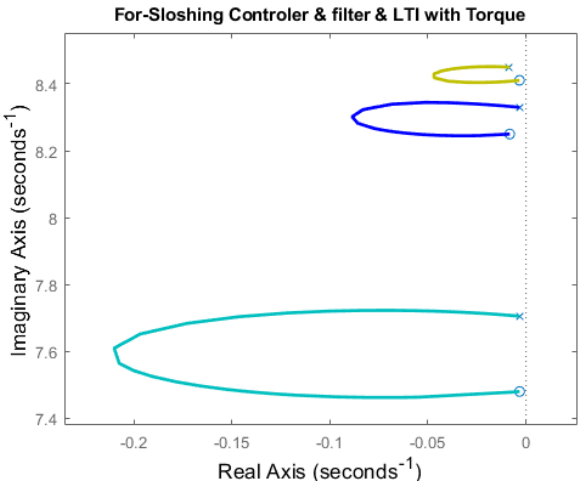

Fig. 12 Root-locus of the controller and filter with LTI containing the torque

where ω_d should be larger than the unstable tank zero frequency, ω_n should be smaller than the unstable tank pole frequency, and $\zeta_n = \zeta_d$. It is remarked that more refined sloshing modes with higher modes may require more complicated filter structures, but for our current phase this one suffices.

For the purpose of this analysis, the filter H(s) was first adjusted to the poles-zeros setting presented in figure 11, yielding the root-locus depicted in figure 12. Hence, the filter was able to address the issue caused by the "closing through the right" root locus, by forcing the poles and zeros of the unstable oxidizer tank to the zeros and poles of the filter. In this case, the closed-loop system remains stable for any feedback gain.

In order to obtain a controller that can stabilize the system, the filter described in eq. (5) was added in the structured robust control design optimization, i.e., the controller gains and the filter parameters were jointly optimized, and the complete uncertain LTI model with the T_{Lx} was used. The gains and filter parameters obtained are presented in figures 13 and 14. The discontinuity present in the figures around t = 80 s is related to the fact that the control effort design weight was reduced for larger ground speeds, in order to attenuate the impact of disturbances during the last few seconds of flight. While no significant transients were observed due to this discontinuity, it is recommended that, as future work, smoother variations between gains are pursued. Figures 15 and 16 illustrate the obtained performance for both tracking error and control effort for the designed controller including the filter, for the nominal system. The controller gains presented here are, hereafter, referred to as "rigid+sloshing controllers".

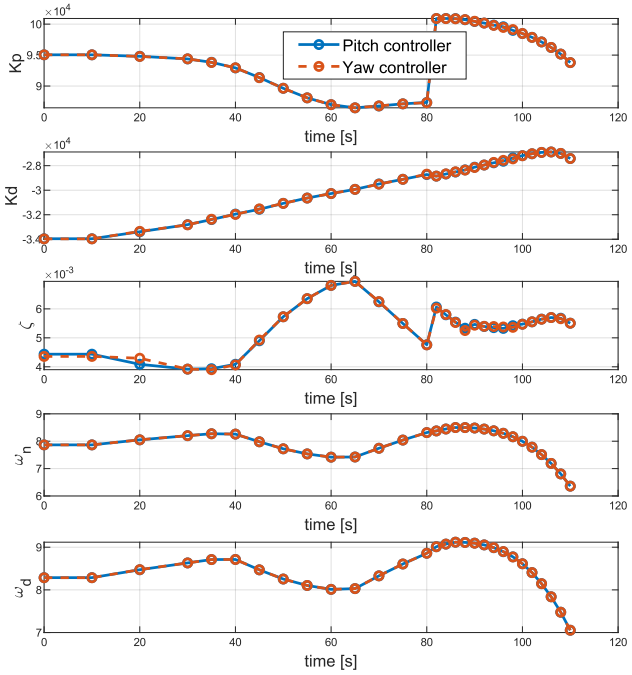

Fig. 13 Pitch and Yaw controller gains and filter parameters for the complete LTI with sloshing

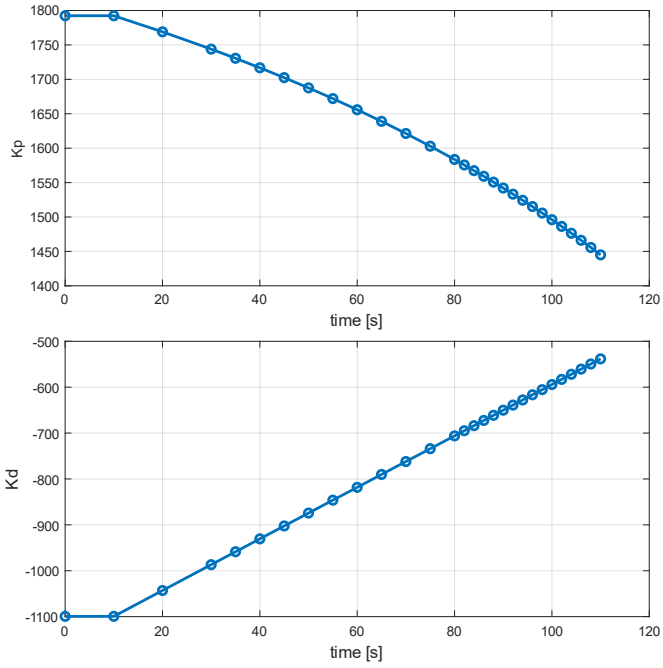

Fig. 14 Roll controller gains for the complete LTI with sloshing

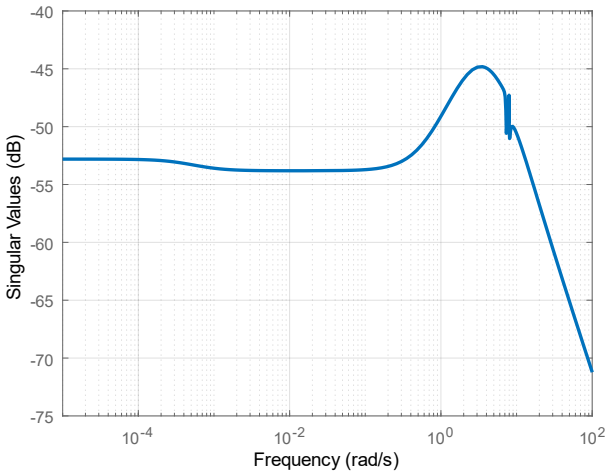

Fig. 15 Singular values of the transfer function from exogenous inputs to tracking error performance considering the PD+filter (pitch & yaw)

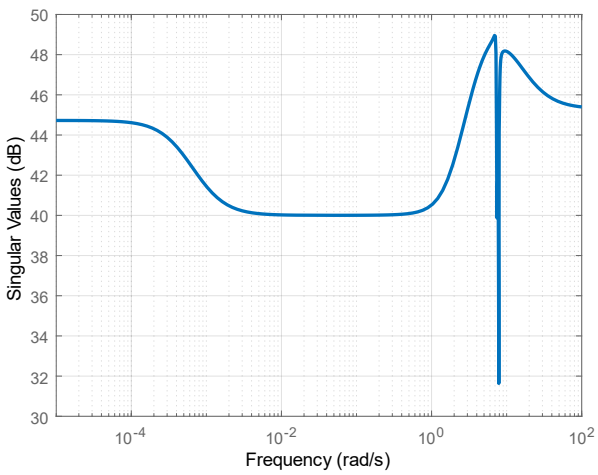

Fig. 16 Singular values of the transfer function from exogenous inputs to control effort considering the PD+filter (pitch & yaw)

The controller implementation in the FES uses LUTs to interpolate the gains and computes the filter matrices in state space format, used to filter the controller commands. In order to minimize the impact of transients due to gain and filter scheduling, the LUT interpolates linearly the gains and the D-methodology is adopted (cf. [9]). The commanded torques are transformed into TVC deflection angles and RCS commands before sending them to the corresponding actuator models.

It is remarked that the TVC dynamics present in the nonlinear FES model, with the exception of the time delay, were neither included in the control design nor in the controller performance analysis, since the TVC model adopted at this early stage of the project may suffer modifications. In particular, the TVC

model adopted corresponds to a worst-case scenario and the usage of such model in the control synthesis and analysis could lead to an over-tailoring of the controller to a pessimistic scenario.

3.3.2 Controller analysis

This section presents the frequency analysis of the rigid+sloshing controller considering the LTI model accounting for the translational, rotational, and sloshing dynamics. Figures 17 to 20 depict the reference to error transfer function, noise to error transfer function, torque disturbance to error transfer function, and the Nyquist diagram, all for the uncertain dynamics in which the uncertainties are the ones used in the LTI. In particular, figures 17 to 19 correspond to 20 randomly generated instances of the transfer functions, provided for illustrative purposes. Regarding the computation of the red disk in figure 20, a total of 500 random instances of the uncertainty system were generated and, for each instantiation, the disk margin was computed. The plotted disk margin corresponds to the smallest disk. The rigid+sloshing controller, composed of the PD gains and the filter, is able to stabilize the complete LTI model, with relatively fast reference tracking capabilities, while minimizing the perturbations introduced by the sloshing dynamics.

The low- and high-frequency gain and delay margins in nominal conditions are presented in table 1, which correspond to the robustness metric considered.

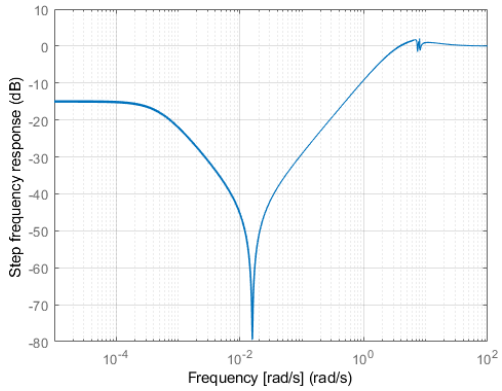

Fig. 17 Reference to error uncertain transfer function

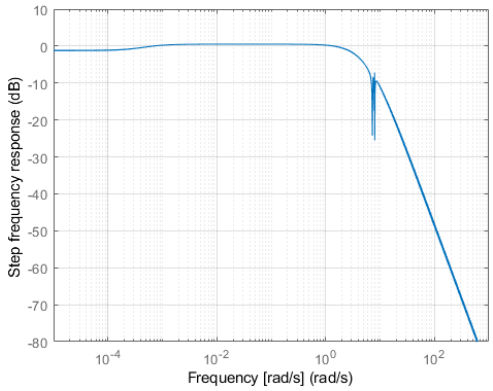

Fig. 18 Noise to error uncertain transfer function

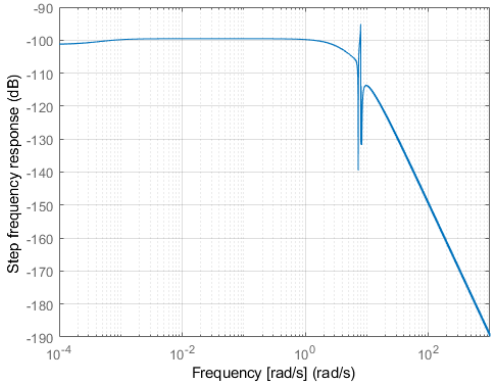

Fig. 19 Torque disturbance to error uncertain transfer function

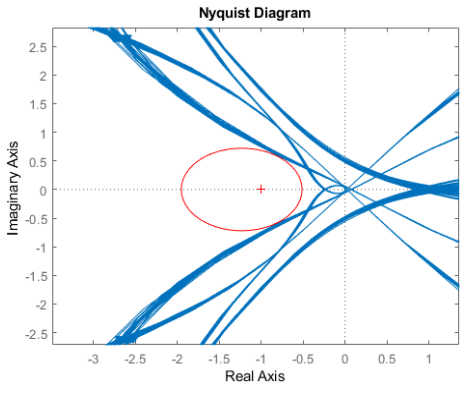

Fig. 20 Uncertain Nyquist diagram, zoom in. The red circle corresponds to the disk margin function

It is remarked that the margins are computed using the system composed of the PD controller with the filter, the total delay using a Padé approximation, and the uncertain rigid+sloshing LTI model. In addition, note that the margins were analyzed for the LTI models at every 10 seconds of the trajectory. It is possible to observe that the gain margins are above the typical requirement value of 6 dB.

Table 1 Gain margins for low and high frequency and minimum phase margins in nominal conditions of the rigid+sloshing controller

Linearization Time [s]	Gain Margin [dB] at Low freq.	Gain Margin [dB] at High freq.	Minimum Delay Margin [ms]
10	50.10	12.54	64.4
20	36.64	12.50	63.8
30	34.12	12.44	63.1
40	35.21	12.43	62.5
50	40.41	12.24	61.2
60	45.23	12.08	59.9
70	40.13	12.15	60.0
80	36.49	12.32	60.7
90	36.19	12.08	56.3
100	37.22	12.10	57.0
110	39.97	11.38	53.7

4 Results

To assess the performance of the overall GNC, considering the rigid+sloshing controller that includes the PD and filter values presented above, a Monte Carlo (MC) campaign was performed composed by 500 runs, dispersing the prescribed uncertainties and perturbation including steady-state wind and moderate turbulence level.

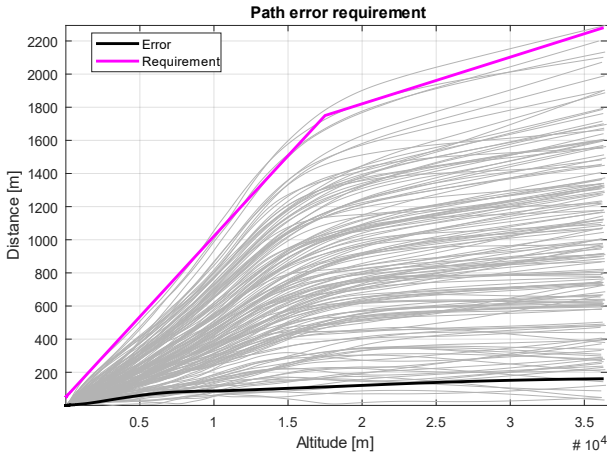

Fig. 21 Flight corridor error

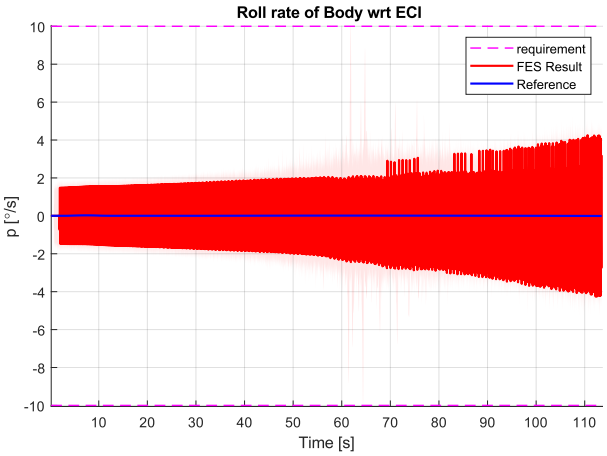

Fig. 22 Roll rate

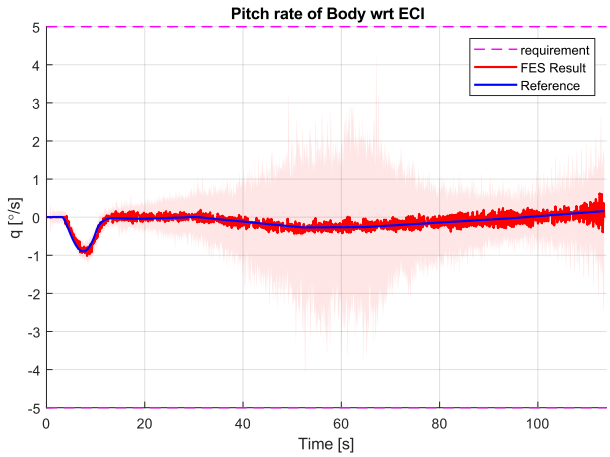

Fig. 23 Pitch rate

Fig. 24 Yaw rate

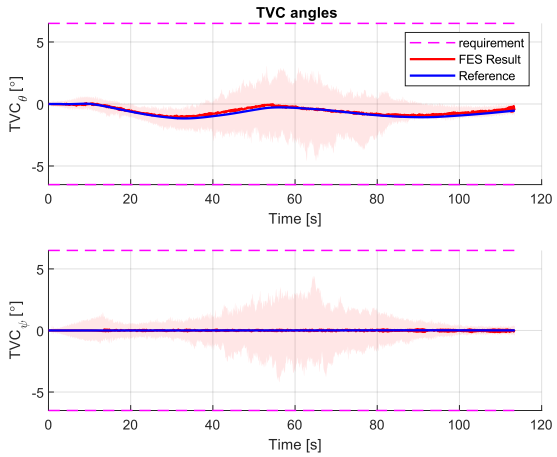

Fig. 25 TVC deflection angles

Figure 21 depicts the flight corridor error, i.e., the norm of the error between the reference position in the ECEF frame and the actual perturbed position obtained with the controller in the loop. All the runs, except 3 out of 500, albeit marginally, satisfy the requirements.

Figures 22 to 24 show the attitude rate and the associated requirement, for which there were no failed runs. Finally, figure 25 shows the TVC deflection angles and it is possible to verify that no run violated the requirement as well.

5 Conclusion

In this paper a PD-like, gain-scheduling, H_∞ robust control approach was adopted for controlling the attitude of the sub-orbital vehicle. The nonlinear model of the vehicle includes several effects such as TVC and RCS nonlinear actuator models between others and, in particular, fuel sloshing, which contributed significantly to making the overall system unstable. To address this problem, an LTI model was developed, including the linearized sloshing dynamics, and used for controller design. The inclusion of the sloshing dynamics in the LTI model not only allowed to assess the sloshing poles location, but also to optimize the parameters of a filter specifically designed to dampen these poles as part of the H_∞ design process. The resulting controller was analyzed and tested in closed-loop with the nonlinear model and the results have demonstrated the requirements satisfaction.

Acknowledgments

The results presented in this paper have been achieved under the Preparation of Enabling Space Technologies and Building Blocks – Phase 2 project led by Omnidea Lda., with ESA contract No. 4000129609/19/NL/BJ. The views expressed in this paper can in no way be taken to reflect the official opinion of the European Space Agency.

References

[1] T. Barrows, J. Orr. *Dynamics and Simulation of Flexible Rockets*. Elsevier, Academic Press, 2021. ISBN: 9780128199947

[2] A. Marcos, D. Navarro-Tapia, P. Simplício, S. Bennani. *Robust Control for Launchers: VEGA Study Case*. Journal of The Society of Instrument and Control Engineers, 2020, Volume 59, Issue 3, Pages 192-202, Released on J-STAGE March 20, 2020, Online ISSN 1883-8170, Print ISSN 0453-4662, DOI: 10.11499/sicejl.59.192, https://www.jstage.jst.go.jp/article/sicejl/59/3/59_192/_article/-char/en

[3] D. Navarro-Tapia, A. Marcos, P. Simplício, S. Bennani, C. Roux. *Legacy recovery and robust augmentation structured design for the VEGA launcher*. International Journal of Robust and Nonlinear Control, 29(11), 3363-3388, 2019. DOI: 10.1002/rnc.4557

[4] T. Afilipoae, A. Neculăescu, P. Simplício, S. Bennani, H. Strauch, *Control Strategies Comparison and Performance Evaluation for a Reusable VTVL Platform based on a Rocket Engine*, The 9th European Conference for Aeronautics and Space Sciences, Lille (France), 27 Jun. - 1 Jul. 2022

[5] H. Bauer. *Fluid Oscillations in the Containers of a Space Vehicle and their Influence upon Stability*. NASA, vol. 187, 1964.

[6] J. Ottander, R. Hall, J. Powers. *Practical Methodology for the Inclusion of Nonlinear Slosh Damping in the Stability Analysis of Liquid-propelled Space Vehicles*. American Institute of Aeronautics and Astronautics, 2018. DOI: 10.2514/6.2018-2097

[7] J. Pei, P. Rothhaar. *Demonstration of Launch Vehicle Slosh Instability on Pole-Cart Platform*. American Institute of Aeronautics and Astronautics, NASA, 2015. DOI: 10.2514/6.2015-2712

[8] J. Adler, M. Lee, J. Saugen. *Adaptive control of propellant slosh for launch vehicles*. Sensors and sensor integration; Proceedings of the Meeting, Orlando,FL,(A93-21961 07-35), 1991. Link: https://ntrs.nasa.gov/citations/19930037966

[9] I. Kaminer, A. M. Pascoal, P. Khargonekar, E. Coleman. *A Velocity Algorithm for the implementation of Gain-scheduled Controller*. Automatica, Vol. 31, No.8, pp. 1185-1191, 1995. DOI: 10.1016/0005-1098(95)00026-S

[10] P. Apkarian. *Tuning controllers against multiple design requirements*. 16th International Conference on System Theory, Control and Computing (ICSTCC) (pp. 1-6). IEEE, 2013. DOI: 10.1109/ACC.2013.6580433